



## ARTICLE

# Pharmacokinetics, mass balance, and metabolism of [<sup>14</sup>C] TPN171, a novel PDE5 inhibitor, in humans for the treatment of pulmonary arterial hypertension

Yi-fei He<sup>1,2</sup>, Yin Liu<sup>1,2</sup>, Jing-hua Yu<sup>1</sup>, Huan Cheng<sup>1,3</sup>, Abdullajon Odilov<sup>1,2</sup>, Fei-pu Yang<sup>1</sup>, Guang-hui Tian<sup>4</sup>, Xiu-mei Yao<sup>4</sup>, Hua-qing Duan<sup>4</sup>, Cheng-yin Yu<sup>5</sup>, Chen Yu<sup>5</sup>, Yan-mei Liu<sup>5</sup>, Gang-yi Liu<sup>5</sup>, Jing-shan Shen<sup>1,2</sup>, Zhen Wang<sup>1,6</sup> and Xing-xing Diao<sup>1,2</sup>

TPN171 is a novel phosphodiesterase-5 (PDE5) inhibitor used to treat pulmonary arterial hypertension (PAH) and erectile dysfunction (ED), which currently is undergoing phase II clinical trials in China. In this single-center, single-dose, nonrandomized, and open design study, radiolabeled [<sup>14</sup>C]TPN171 was used to investigate the metabolic mechanism, pharmacokinetic characteristics, and clearance pathways of TPN171 in 6 healthy Chinese male volunteers. Each volunteer was administered a single oral suspension of 10 mg (100 μCi) of [<sup>14</sup>C]TPN171. We found that TPN171 was absorbed rapidly in humans with a peak time ( $T_{max}$ ) of 0.667 h and a half-life ( $t_{1/2}$ ) of approximately 9.89 h in plasma. Excretion of radiopharmaceutical-related components was collected 216 h after administration, accounting for 95.21% of the dose (46.61% in urine and 48.60% in feces). TPN171 underwent extensive metabolism in humans. Twenty-two metabolites were detected in human plasma, urine, and feces using a radioactive detector combined with a high-resolution mass spectrometer. According to radiochromatograms, a glucuronide metabolite of *O*-dealkylated TPN171 exceeded 10% of the total drug-related components in human plasma. However, according to the Food and Drug Administration (FDA) guidelines, no further tests are needed to evaluate the safety of this metabolite because it is a phase II metabolite, but the compound is still worthy of attention. The main metabolic biotransformation of TPN171 was mono-oxidation (hydroxylation and *N*-oxidation), dehydrogenation, *N*-dealkylation, *O*-dealkylation, amide hydrolysis, glucuronidation, and acetylation. Cytochrome P450 3A4 (CYP3A4) mainly catalyzed the formation of metabolites, and CYP2E1 and CYP2D6 were involved in the oxidative metabolism of TPN171 to a lesser extent. According to the incubation data, M1 was mainly metabolized to M1G by UDP-glucuronosyltransferase 1A9 (UGT1A9), followed by UGT1A7 and UGT1A10.

**Keywords:** TPN171; [<sup>14</sup>C]TPN171; PDE5 inhibitor; pulmonary arterial hypertension; healthy volunteers; pharmacokinetics; metabolite identification; mass balance

*Acta Pharmacologica Sinica* (2022) 0:1–13; <https://doi.org/10.1038/s41401-022-00922-6>

## INTRODUCTION

TPN171 is a new pyrimidinone phosphodiesterase-5 (PDE5) inhibitor jointly developed by Shanghai Institute of Materia Medica, Chinese Academy of Sciences, and Vigonvita Life Sciences Co., Ltd [1]. This compound is clinically intended to treat pulmonary arterial hypertension (PAH) and male erectile dysfunction (ED). TPN171 showed good safety and pharmacokinetic profiles in phase I studies [2]. In China, a phase IIa study in patients with PAH (ClinicalTrials.gov Identifier: NCT04483115) and a phase III study in patients with ED (ClinicalTrials.gov Identifier: NCT05188989) were underway at the time this paper was written [3].

PAH is a progressive pulmonary vascular disease that may involve various clinical conditions and the most complicated cardiovascular and respiratory diseases [4], and its main pathophysiological feature is an increase in pulmonary artery pressure in

the resting state. PAH causes the lips to appear blue–purple in color, which are called “blue lips” [5, 6]. If not actively treated, most patients with PAH will die of right heart failure within 2 to 3 years, and thus the disease is also called a “malignant tumor of the cardiovascular system” [7]. PAH is a rare disease in European and American countries, and idiopathic pulmonary hypertension is listed first in China’s rare disease list. In other words, PAH is a severe chronic and life-threatening disease [8].

PDE5 is mainly distributed in the corpora cavernosa of the penis and the pulmonary vascular system and is a major cGMP-hydrolyzing enzyme expressed in all types of smooth muscle. Selective PDE5 inhibitors potentiate the relaxant effect of the neurotransmitter NO by increasing cGMP accumulation in smooth muscle cells, thereby causing smooth muscle relaxation. In addition, NO induces a large number of smooth muscle cells to enter the corpus cavernosum of the penis, causing smooth muscle

<sup>1</sup>State Key Laboratory of Drug Research, Shanghai Institute of Materia Medica, Chinese Academy of Sciences, Shanghai 201203, China; <sup>2</sup>University of the Chinese Academy of Sciences, Beijing 100049, China; <sup>3</sup>School of Pharmaceutical Sciences, Shandong University of Traditional Chinese Medicine, Ji-nan 250355, China; <sup>4</sup>Vigonvita Life Sciences Co., Ltd, Suzhou 215000, China; <sup>5</sup>Shanghai Xuhui Central Hospital, Shanghai 200030, China and <sup>6</sup>Lingang Laboratory, Shanghai 201602, China

Correspondence: Zhen Wang (wangzhen@lglab.ac.cn) or Xing-xing Diao (xxdiao@simm.ac.cn)

These authors contributed equally: Yi-fei He, Yin Liu

Received: 31 December 2021 Accepted: 11 May 2022

Published online: 08 June 2022

relaxation, the expansion of the corpus cavernosum, entry of a large amount of blood entering the penis that produces an erection, and curing male ED and other diseases [9]. However, human PDE contains 11 subfamilies (PDE1-PDE11) that hydrolyze the ubiquitous second messenger cGMP or cyclic adenosine monophosphate (cAMP) [10, 11].

Both sildenafil and tadalafil have been approved by the Food and Drug Administration (FDA) as treatments for PAH [12]. These drugs did not exert a greater inhibitory effect on PDE5 than on PDE6 and PDE11. Unsatisfactory selectivity across multiple PDEs may lead to excessive side effects, limiting their clinical application [13, 14]. Therefore, new high-efficiency and low-toxicity PDE5 inhibitors may provide excellent application prospects for PAH treatment.

The TPN171 research team discovered flavonoids with high PDE5 inhibitory activity in the extract of the traditional Chinese medicine *Epimedium*. After the evaluation of selectivity, liver microsomal metabolic stability, and drug efficacy in animals, TPN171 was finally determined to be a candidate drug [1]. TPN171 showed more robust PDE5 inhibitory activity ( $IC_{50} = 0.62$  nM) than sildenafil ( $IC_{50} = 4.31$  nM) and tadalafil ( $IC_{50} = 2.35$  nM) in an in vitro activity test. Compared with PDE6 (related to visual side effects), the selectivity of TPN171 was 32 times higher, and was better than sildenafil (8 times); compared with PDE11, the selectivity of TPN171 reached 1610 times, which was significantly better than tadalafil (9 times) [15, 16]. Oral TPN171 administration substantially reduces the mean pulmonary artery pressure in rats with monocrotaline-induced PAH, and the effective dose is much lower than that of sildenafil [1].

Although TPN171 has shown potential as a first-line drug and has been investigated in numerous studies, its metabolic fate in humans is unclear. Determining the metabolites of TPN171, evaluating the safety of its metabolites, understanding its pharmacokinetics, and determining its clearance mechanism are very important to understand its behavior in humans [17]. The use of radiotracers, such as <sup>14</sup>C-labeled compounds, in absorption, distribution, metabolism, and excretion studies has enabled researchers to determine the mass balance and main metabolic pathways of drug candidates [18–22].

Radioisotope tracing technology has the obvious advantages of strong specificity and the ability to fully track the in vivo behavior of drugs. Radiolabeling technology is considered the “gold standard” for the analysis of mass balance, tissue distribution, and metabolite profiles. This technique quantitatively reflects the proportions of metabolites, obtains the excretion pathways of drugs, clarifies the main biotransformation pathways of medicines in the body, effectively identifies whether disproportionate metabolites are present in human blood circulation, and provides robust evidence for evaluating potential drug–drug interactions.

The results from the completed clinical trial (ClinicalTrials.gov Identifier: NCT04479917) and preliminary research data from this product suggested that 10 mg was a potentially effective dose and that the drug was safe and well-tolerated at this dose. Therefore, in this study, 6 healthy Chinese male volunteers were administered a suspension of 10 mg (100 μCi) of [<sup>14</sup>C]TPN171. By measuring the radioactivity in the volunteers’ blood and plasma, the pharmacokinetics of [<sup>14</sup>C]TPN171 in the blood and plasma were investigated, and quantitative analysis was conducted. Mass balance data and main excretion pathways were obtained by measuring the radioactivity in urine and feces. In addition, various in vitro metabolic models were used to investigate the mechanism underlying the formation of primary metabolites.

## MATERIALS AND METHODS

### Chemicals and reagents

TPN171H tablets were provided by Vigonvita Life Sciences Co., Ltd (Suzhou, China). [<sup>14</sup>C] TPN171H (content: 97.49%) was provided by

Wuxi Beta Pharmaceutical Technology Co., Ltd (Wuxi, China). Reference substances of TPN171 (content: 99.79%) and its metabolites M1 (content: 87.99%), M2 (content: 95.16%), M3-1 (content: 91.91%), M3-2 (content: 99.79%), M3-3 (content: 97.49%), M6 (content: 98.96%), M7-3 (content: 88.33%) and TPN171M1G (content: 95%) were synthesized in house, and their identities, contents and purities were assessed using nuclear magnetic resonance spectroscopy, mass spectrometry, and high-performance liquid chromatography (Fig. 1).

Human liver microsomes (HLMs) and human kidney microsomes (HKMs) were purchased from SEKISUI Xenotech (Kansas City, KS, USA). Human intestinal microsomes (HIMs) and human smoked lung microsomes (HSLMs) were purchased from the Research Institute for Liver Diseases Co., Ltd (Shanghai, China). Recombinant human cytochrome P450 (CYP450) enzymes (CYP1A2, CYP1B1, CYP2A6, CYP2B6, CYP2C8, CYP2C9, CYP2C19, CYP2D6, CYP2E1, CYP3A4, CYP3A5, and CYP4A11) and recombinant human UDP-glucuronosyltransferase (UGT) enzymes (UGT1A1, UGT1A3, UGT1A4, UGT1A6, UGT1A7, UGT1A8, UGT1A9, UGT1A10, UGT2B4, UGT2B7, UGT2B10, UGT2B15, and UGT2B17) were all purchased from Corning Gentest (Glendale, AZ, USA). Uridine 5'-diphosphoglucuronic acid (UDPGA) was purchased from Merck Limited (Shanghai, China). Tris-HCl, niflumic acid, and phenacetin were purchased from Meilunbio (Dalian, China), and the liquid scintillation cocktail was obtained from Zhejiang Dingxin Technology Co., Ltd (Zhuji, China).

### Instrumental conditions

In this study, high-resolution mass spectrometry (HR-MS) data were acquired using a Vanquish ultrahigh-performance liquid chromatography (UHPLC) system combined with a Q Exactive Plus mass spectrometer (Thermo, Waltham, MA, USA). Chromatographic separation was achieved on an ACE Excel 3 C18-AR column (3 μm, 100 mm × 2.1 mm) with a Phenomenex Krud-Katcher Ultra HPLC In-Line Filter guard column (2 μm, Depth Filter × 0.004 ID). The column temperature was 40 °C, and the flow rate was 0.45 mL/min. The mobile phase consisted of a 2 mM aqueous ammonium acetate solution containing 0.1% formic acid (A) and acetonitrile (B). The gradient elution procedure was as follows: 0 min, 10% B; 2 min, 10% B; 42 min, 60% B; 44 min, 95% B; 47 min, 95% B; 47.1 min, 10% B; and 50 min, 10% B. The eluent was monitored using ultraviolet (UV) spectroscopy at a wavelength of 254 nm. The mass spectrometer was operated in positive electrospray ionization (ESI) mode with an  $m/z$  80–1000 Da scanning range for detection. The optimized MS parameters were as follows: sheath gas, 45 L/min; auxiliary gas, 10 L/min; normalized collision energy, 30, 40, and 50; capillary temperature, 320 °C; auxiliary gas heater temperature, 400 °C; and capillary voltage, 3.5 kV. Data were collected using Xcalibur software (Thermo) and analyzed using Compound Discoverer software (Thermo).

### Study design, dosing, and sample collection

This study employed a single-center, single-dose, nonrandomized and open design (ClinicalTrials.gov Identifier: NCT04655872) with the plan to enroll six healthy Chinese male volunteers at Shanghai Xuhui Central Hospital (Shanghai, China). Based on the human dosimetry analysis, a trial protocol was drafted together with the hospital and was approved by the hospital ethics committee. Each volunteer took a single oral suspension containing 10 mg (100 μCi) of [<sup>14</sup>C]TPN171 after an overnight fast. Pharmaceutical grade saline was used to dissolve [<sup>14</sup>C]TPN171H. After aliquoting, each volunteer’s dosing solution contained 100 μCi of [<sup>14</sup>C]TPN171, and then 10 mg of TPN171H tablets and ultrapure water were added to a total volume of 40 mL.

Biological samples were collected from 6 healthy Chinese male volunteers from 0 to 216 h, including blood, plasma, urine, and feces. The specific sample collection time points or periods are described below.

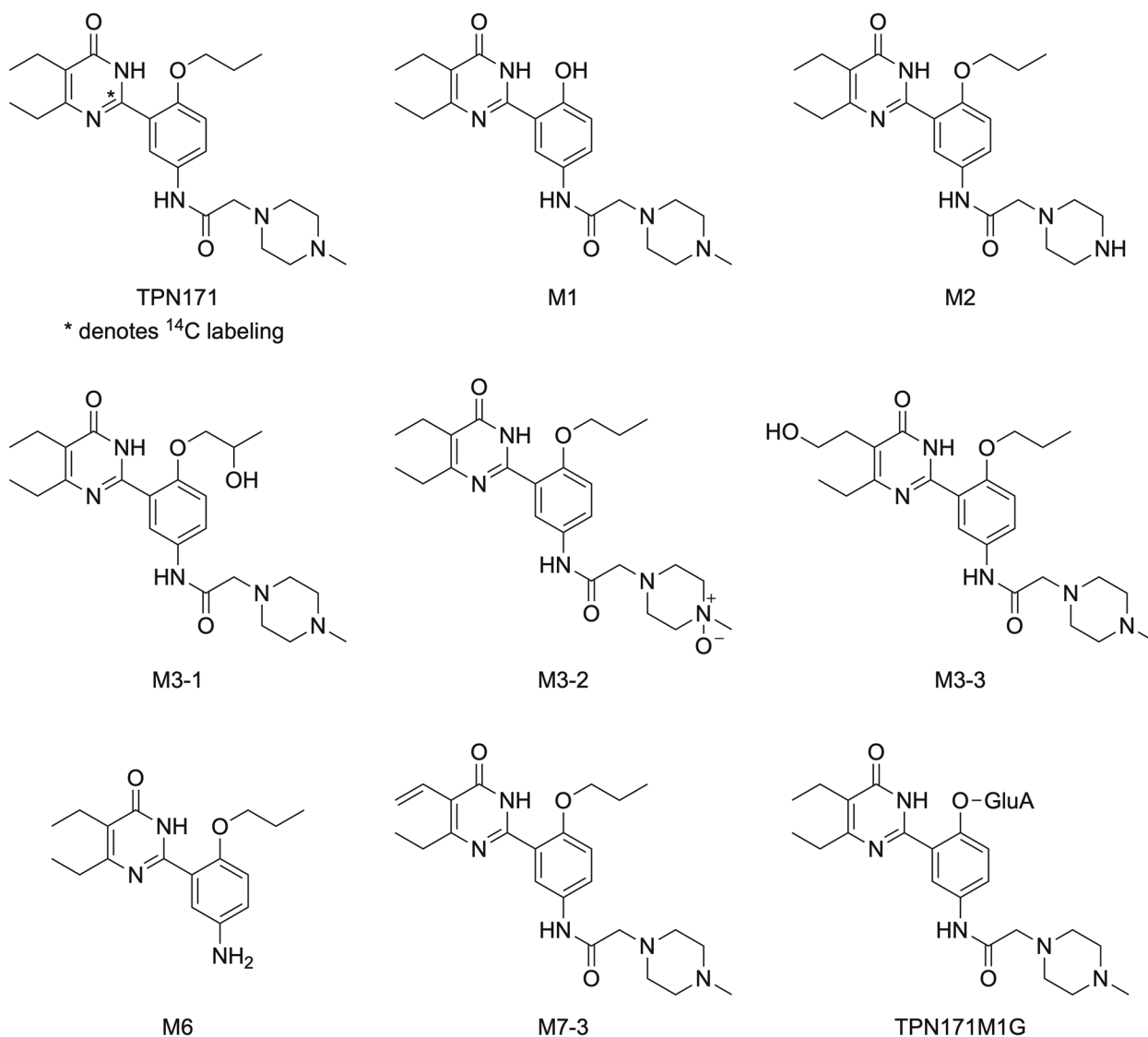


**Fig. 1** Chemical structures of TPN171 and 8 reference metabolites.

Blood samples were collected within 1 h before administration and 0.5, 0.75, 1, 1.5, 2, 4, 6, 8, 10, 12, 24, 48, 72, 96, 120, 168, and 216 h after administration. Approximately 7 mL of venous blood was collected at each time point in heparin anticoagulant-containing blood collection tubes. The centrifugal separation of plasma was mainly used for nonradioactive and radioactive pharmacokinetics analyses and the biotransformation analysis. In addition, approximately 10 mL of additional venous blood was collected within 1 h before administration and 1, 4, 10, 12, 24, and 48 h after administration, of which 2 mL was aliquoted for the analysis of total radioactivity in blood; the remaining blood was centrifuged to obtain plasma and used for the biotransformation analysis. Blood and plasma samples were frozen and stored at  $-90^{\circ}\text{C}$  to  $-60^{\circ}\text{C}$ .

A urine sample was randomly collected before drug administration and all urine was collected at 0–4, 4–8, 8–24, 24–48, 48–72, 72–96, 96–120, 120–144, 144–168, 168–192, and 192–216 h after administration. A feces sample was randomly collected before drug administration and all feces were collected at 0–24, 24–48, 48–72, 72–96, 96–120, 120–144, 144–168, 168–192, and 192–216 h after administration. When the total radioactivity of the biological sample (urine + feces) collected by each volunteer exceeded 80% of the dose, the collected radioactivity was less than 1% of the dose for two consecutive time intervals, and the radioactivity of plasma at 2 consecutive time points

was lower than 3 times the radioactivity at 0 h before administration, we terminated the collection of urine and feces.

#### Analysis of total radioactivity

Levels of radioactivity in human plasma and urine samples was determined by counting aliquots directly in a liquid scintillation counter (LSC, Hidex, Finland). The evolved <sup>14</sup>CO<sub>2</sub> from feces and blood combusted in a biological sample oxidizer was captured in 15 mL of alkaline liquid scintillation cocktail. Samples were analyzed in duplicate to produce extraction data (direct counting). Sample radioactivity was assayed with an LSC for 5 min or until the 2-sigma error was reached, whichever occurred first. The LSC was programmed to automatically subtract the instrument background (including cocktail) and convert counts per minute (CPM) to disintegrations per minute (DPM).

#### Sample preparation for metabolite radioprofiling

**Plasma.** According to the radiopharmacokinetic concentration results, the plasma samples collected before drug administration and 0.5, 0.75, 1, 1.5, 2, 4, 6, 8, 10, 12, and 24 h after administration were pooled individually based on the AUC-pooling principle [23]. The plasma samples were mixed in equal volumes to obtain an AUC<sub>0–24 h</sub> pooled plasma sample.

**Table 1.** Samples selection for radioprofiling and recovery of radioactivity from extracted and reconstituted samples.

Matrix	Time points/intervals (h)	Extraction/centrifugation recovery (%) <sup>a</sup>	Reconstitution recovery (%)
Plasma <sup>b</sup>	0, 0.5, 0.75, 1, 1.5, 2, 4, 6, 8, 10, 12, 24	111.14	90.15
Urine <sup>c</sup>	0–4, 4–8, 8–24, 24–48	94.87	98.64
Feces <sup>d</sup>	0–24, 24–48, 48–72, 72–96	97.21	90.17

<sup>a</sup>The plasma and fecal samples were extracted with methanol/acetonitrile (50:50, v/v) and water. The urine samples were centrifuged to remove solids.

<sup>b</sup>The plasma samples were individually pooled according to the AUC-pooling principle, and then an equal volume from individuals of the same sex was pooled together.

<sup>c</sup>An equal percentage of volume was pooled. Notably, 0–48 h urine radioactivity accounted for more than 90% of total urine radioactivity based on cumulative radioactivity recorded at 0–216 h post-dose; thus, 0–48 h urine samples were pooled.

<sup>d</sup>Equal percentages of the weight of selected samples were pooled. In this experiment, 0–96 h feces radioactivity accounted for more than 90% of total fecal radioactivity according to cumulative radioactivity measured for 0–216 h post-dose; thus, 0–96 h feces samples were pooled.

**Urine.** According to the cumulative radioactivity measured from 0–216 h post-dose, radioactivity in the 0–48 h urine samples accounted for more than 90% of total urine radioactivity. Based on the urine sample volume collected from 6 subjects in each period, the corresponding amounts of 0–4, 4–8, 8–24, and 24–48 h urine samples were collected in equal percentages and pooled to obtain 0–48 h urine samples.

**Feces.** According to the cumulative radioactivity measured for 0–216 h post-dose, 0–96 h fecal radioactivity accounted for more than 90% of the total fecal radioactivity. Based on the feces sample weight of 6 subjects in each period, the corresponding amounts of 0–24, 24–48, 48–72, and 72–96 h feces were collected in equal percentages and pooled to obtain 0–96 h fecal samples.

The pooled plasma and fecal samples were extracted by adding three volumes of methanol/acetonitrile (50:50, v/v). The mixture was shaken (1 min) and sonicated (5 min) three times before centrifugation (5000 rpm, 10 min). The supernatant was transferred to a clean tube, and then 0.5 volume of water and one volume of methanol/acetonitrile (50:50, v/v) were added to the postextraction solid. The mixture was shaken (1 min) and sonicated (5 min) three times before centrifugation (5000 rpm, 10 min). The two supernatants were combined, and the extraction recovery was measured. The pooled urine sample was centrifuged (5000 rpm, 10 min), and the recovery was measured after centrifugation.

Then, the supernatant was concentrated under nitrogen and reconstituted with 0.1% formic acid in an ethanol-water (20:80, v/v) solution. The reconstitution recovery was calculated after measuring the radioactivity of the reconstituted solution. The recoveries of pooled plasma, urine, and fecal samples are described in detail in Table 1.

#### Radioprofiling

Due to the low radioactivity of human plasma and feces, fractions were collected using a UHPLC fraction collector (Thermo) over time (8 s/fraction) in Deepwell LumaPlate™ 96-well plates. After evaporation, the radioactivity was determined with an offline Sense Beta detector (Hidex). For the urine samples, the UHPLC eluent was analyzed using an online radioactivity detector (β-RAM).

Radioactive metabolite profiling was integrated to obtain the radiochromatogram using Laura software (Lablogic, UK). The percentage of each metabolite in urine and feces (% dose) and the ratio of metabolites in the plasma after exposure (% area under the curve, %AUC) were calculated.

#### Metabolite identification

The structures of metabolites were identified using UHPLC-Q Exactive Plus MS. The mass spectral fragmentation patterns of metabolites were compared with the precursor compound and

other available reference substances, which provided a solid foundation for the characterization of unknown metabolites. The molecular ion peaks corresponding to the prominent radioactive chromatographic peaks were analyzed. Fragment ions were generated by performing a product ion scan.

#### Pharmacokinetics analysis

The total radioactive concentrations in blood and plasma were measured with an oxidation combustor and LSC. Quantitative determination of TPN171 levels in plasma and blood at different time points was performed using a validated LC–MS/MS method. TPN171 was quantitated on a Triple Quad 6500 mass spectrometer (Sciex, Framingham, MA, USA) coupled with a 30 A HPLC system (Shimadzu, Kyoto, Japan). The quantitative transition ion pairs were  $m/z$  442 → 113. The calibration curves were linear over the plasma concentration ranges of 0.500–1000 ng/mL for TPN171. The lower limit of quantification for TPN171 was 0.500 ng/mL. The pharmacokinetics parameters were estimated with WinNonlin software based on the concentration of TPN171 in the blood and plasma. The ratio of the total radioactive substance concentration in blood and plasma was calculated to evaluate the preferred distribution preference in blood and plasma.

#### Mass balance

The total radioactivity in urine and feces was measured using LSC and an oxidation combustor. According to the weight of urine and feces collected at each time interval and the measured radioactivity concentration, the excretion of [<sup>14</sup>C]TPN171-related components was calculated, and the excretion rate and main excretion route were evaluated.

#### Incubation of TPN171 with HLMs and recombinant CYP450s

The volume of the incubation system was 200 μL, and the buffer solution was 50 mM Tris-HCl (pH 7.4), including a final concentration of 3 μM TPN171, 8 mM MgCl<sub>2</sub>, and 2 mM NADPH. The incubation was performed in a 37 °C water bath. After preincubation for 3 min, the recombinant protein or the chemical inhibitor was added to the buffer-substrate-cofactor mixture to initiate the reaction. The protein concentration of HLMs or recombinant CYP450s was 0.5 mg/mL. The chemical inhibitors were 1-aminobenzotriazole (ABT, inhibitor of all CYP450s) [24] and ketoconazole (CYP3A4/5 inhibitor) [25]. After 60 min, the reaction was terminated by adding 200 μL of ice-cold acetonitrile.

#### TPN171M1 O-glucuronidation by HLMs, HKMs, HIMs, HSLMs, and recombinant UGTs

The volume of the incubation system was 200 μL, and the buffer solution was 50 mM Tris-HCl (pH 7.4), including a final concentration of 3 μM M1, 8 mM MgCl<sub>2</sub>, 25 μg/mL alamethicin, and 2 mM UDPGA. The incubation was performed in a 37 °C water bath. After preincubation for 3 min, the recombinant

protein or the chemical inhibitor was added to the buffer-substrate-cofactor mixture to initiate the reaction. The protein concentration of HLMs, HKMs, HIMs, HSLMs, and recombinant UGTs was 0.5 mg/mL. The chemical inhibitors were niflumic acid (UGT1A9 inhibitor) [26] and tolcapone (UGT1A7/UGT1A10 inhibitor) [27]. After 60 min, the reaction was terminated by adding 200  $\mu$ L of ice-cold acetonitrile.

#### Statistical analysis

The radioactive dose recovery, cumulative radioactive recovery in urine, feces, and bile, and radioactive concentration in plasma were performed using Microsoft<sup>®</sup> Excel. Pharmacokinetic parameters were performed with WinNonlin (Version 7.0, Certara, USA). In the calculation of pharmacokinetic parameters, the concentration below the lower limit of quantification (BQL) before  $T_{max}$  was calculated as "0", and after that, it was treated as a missing value. In descriptive statistical analysis, it is calculated as "0".

## RESULTS

### HR-MS analysis of reference standards of TPN171 and its metabolites

First, HR-MS was performed on a solution of reference substances of TPN171 and 8 metabolites (1.00  $\mu$ g/mL) to determine their mass fragmentation patterns and chromatographic behaviors.

**TPN171.** Under the experimental conditions used in this study, the retention time of TPN171 (C<sub>24</sub>H<sub>35</sub>N<sub>5</sub>O<sub>3</sub>) was 37.88 min, and a molecular ion ([M + H]<sup>+</sup>) at  $m/z$  442.2804 was obtained in full-scan MS. In the product ion scan, the primary fragment ions obtained were  $m/z$  314.1867, 286.1186, 259.1315, 244.1206, 113.1073, 98.0838, and 70.0651 (Fig. 2a). The fragment ion at  $m/z$  314.1867 was formed by loss of the piperazine moiety and CO. The fragment ion at  $m/z$  259.1315 was produced through cleavage of the amide bond. The fragment ion at  $m/z$  113.1075 was the removed piperazine moiety.

**M1.** M1 was the *O*-depropylated product of TPN171 and had a retention time of 35.25 min ([M + H]<sup>+</sup>  $m/z$  400.2343). The major fragment ions of M1 were  $m/z$  113.1076, 98.0841, and 70.0657, which were the same as those of TPN171 (Fig. 2b).

**M2.** M2 was the *N*-demethylated product of TPN171, and its retention time was 35.12 min ([M + H]<sup>+</sup>  $m/z$  428.2656). The major fragment ions were  $m/z$  99.0919 and 70.0657. The fragment ion at  $m/z$  99.0919 was the removed piperazine moiety. The fragment ion  $m/z$  70.0657 was the same as that of TPN171 (Fig. 2c).

**M3-1, M3-2, and M3-3.** M3-1 to M3-3 were mono-oxidated metabolites of TPN171 at different positions. Their molecular ion [M + H]<sup>+</sup> was  $m/z$  458.2751.

M3-1 was the product of TPN171 hydroxylated on the *O*-side chain with a retention time of 29.09 min. The major fragment ions of M3-1 were  $m/z$  113.1075 and 70.0656, which were the same as those of TPN171 (Fig. 2d).

M3-2 was the product of TPN171 *N*-oxidated on the piperazine group, and its retention time was 33.55 min. The major fragment ions of M3-2 were  $m/z$  328.1651, 286.1183, 113.1075, 98.0841, and 70.0656. The fragment ion at  $m/z$  328.1651 was formed by the loss of the piperazine moiety and O atom. The other fragment ions were the same as those of TPN171 (Fig. 2e).

M3-3 was the product of TPN171 hydroxylated on the side chain of the pyrimidine moiety, and its retention time was 28.30 min. The major fragment ions of M3-3 were  $m/z$  113.1076 and 70.0657, which were the same as those of TPN171 (Fig. 2f).

**M6.** M6 was the amide hydrolysis product of TPN171, and its retention time was 35.01 min ([M + H]<sup>+</sup>  $m/z$  302.1857). The major

fragment ion at  $m/z$  259.1266 was produced through cleavage of the amide bond (Fig. 2g).

**M7-3.** M7-3 was the reduced product of TPN171, and its retention time was 39.56 min ([M + H]<sup>+</sup>  $m/z$  440.2648). The major fragment ions of M7-3 were  $m/z$  113.1075 and 70.0657, which were the same as those of TPN171 (Fig. 2h).

**TPN171M1G.** TPN171M1G was a glucuronide of M1 with a retention time of 28.46 min ([M + H]<sup>+</sup>  $m/z$  576.2656), and its major fragment ions were  $m/z$  400.2331, 113.1075, and 70.0656. These fragment ions were the same as those of M1 (Fig. 2i).

### Pharmacokinetics and mass balance of TPN171

As shown in Table 2, after a single oral administration of [<sup>14</sup>C] TPN171 to 6 healthy Chinese male volunteers, TPN171 was absorbed rapidly in humans, with a peak time ( $T_{max}$ ) of 0.667 h and a half-life ( $t_{1/2}$ ) of 9.89 h (Fig. 3a) in human plasma. The geometric mean of plasma exposure (AUC<sub>0-∞</sub>) was 480 h·ng/mL. The concentration of drug-related components began to fall below the limit of quantification (BQL, which is three times the radioactive concentration in plasma before administration) 48 h after administration.

In humans, excreted radioactivity time profiles in urine and feces were similar following a single oral administration of a 10 mg (100  $\mu$ Ci) [<sup>14</sup>C]TPN171 suspension (Fig. 3b). The majority of radioactivity was excreted within 96 h after administration, accounting for 92.05% of the dose. Within 216 h after administration, the cumulative excretion of radiopharmaceutical-related components in urine and feces was 95.21% of the dose (46.61% of the dose in urine and 48.60% of the dose in feces).

### Radioprofiling and metabolite identification

Unmetabolized TPN171 was detected as a major component in human plasma, urine, and feces. In addition, 22 metabolites were identified. The radioactive distribution of TPN171 and its metabolites in human plasma, urine, and feces and the percent of the dose in urine and feces are shown in Table 3.

**Plasma.** In human plasma, the radioactivity of TPN171 and identified metabolites accounted for 95.12% of the total exposure; TPN171 accounted for 42.35% of exposure. Combined with the HR-MS analysis, 12 metabolites were detected in plasma, of which TPN171M1G was the most abundant metabolite, accounting for 14.14% of the total exposure; M457-1 was the second most abundant metabolite, accounting for 7.05% of the total exposure (Fig. 4a).

M457-1 was the third most abundant metabolite, accounting for 7.05% of the total exposure. The chromatographic retention time of M457-1 was 31.29 min, and the molecular ion ([M + H]<sup>+</sup>) of  $m/z$  458.2755 was obtained in full-scan MS. According to the exact mass, the molecular formula was C<sub>24</sub>H<sub>35</sub>N<sub>5</sub>O<sub>4</sub>, indicating that an O atom was added to the parent drug. The major fragment ions were  $m/z$  440.2650, 113.1076, and 70.0657. The fragment ion at  $m/z$  440.2650 was obtained from the neutral loss of one molecule of water from the precursor ion, and the other fragment ions were the same as those of the parent drug. M457-1 was speculated to be the mono-oxidation product of TPN171. M3-1, M3-2, M3-3, and M457-1 were isomers (Fig. 5a).

**Urine.** The total radioactive components excreted in human urine accounted for 46.61% of the dose, and TPN171 accounted for 19.66% of the dose. Combined with the HR-MS analysis, 21 metabolites were detected, of which M575-1 was the most abundant metabolite, accounting for 9.33% of the dose; M2 and M6 (coeluting) were the second most abundant metabolites, accounting for 4.95% of the dose. M455-1 and M455-2 (coeluting) accounted for 2.90% of the dose (Fig. 4b).

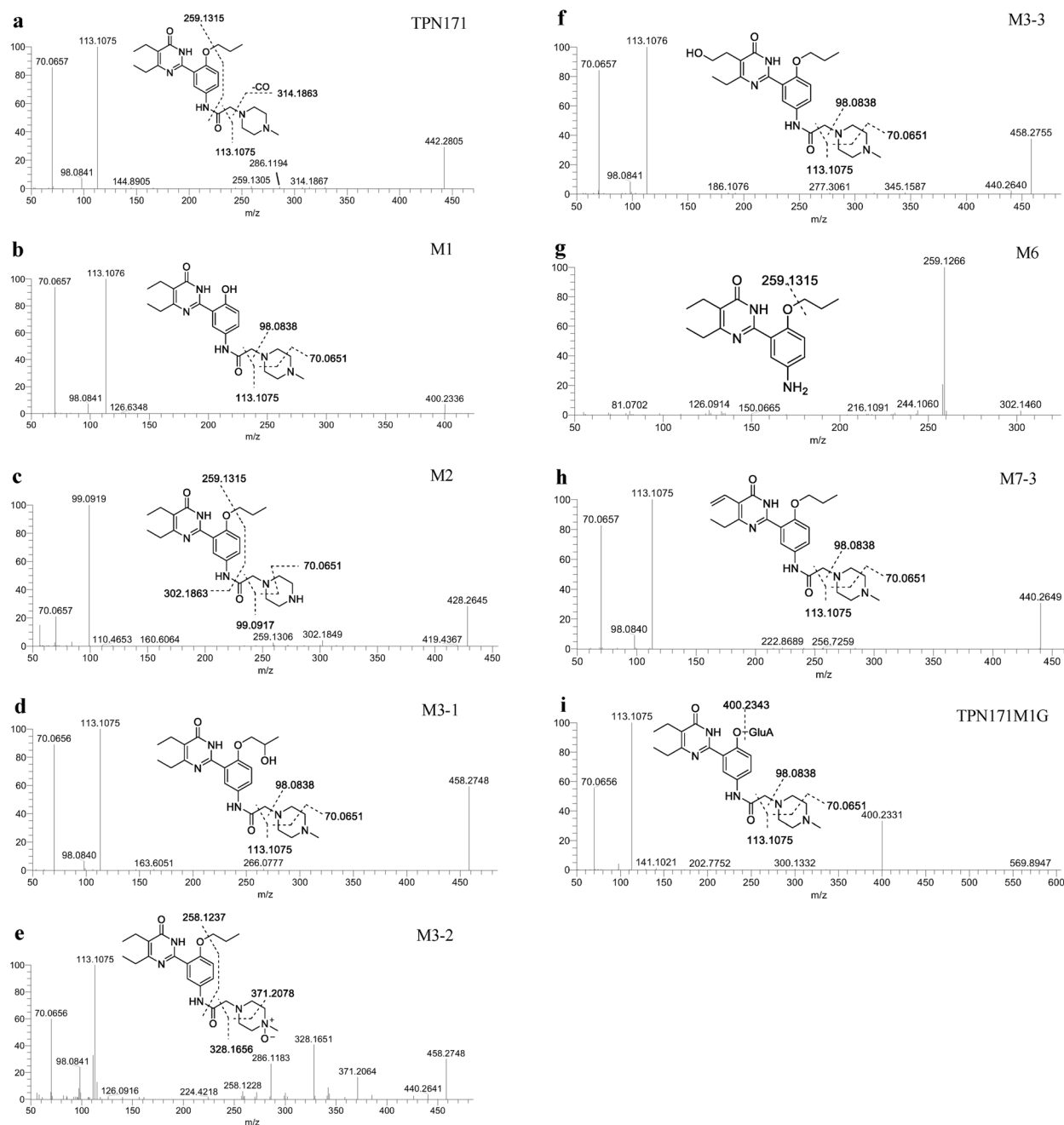


**Fig. 2** Product ion spectra and proposed fragmentation patterns of reference substances. TPN171 (a), M1 (b), M2 (c), M3-1 (d), M3-2 (e), M3-3 (f), M6 (g), M7-3 (h), and TPN171M1G (i).

The retention time of M575-1 was 11.67 min, and the molecular ion ( $[M + H]^+$ )  $m/z$  576.2653 was obtained in full-scan MS. According to the exact mass, the molecular formula of M575-1 was  $C_{27}H_{37}N_5O_9$ , which was M1 with the addition of  $C_6H_8O_9$ . The major fragment ions at  $m/z$  400.2336, 113.1077, and 70.0658 were the same as those of M1. M575-1 was speculated to be a glucuronide of M1, an isomer of TPN171M1G (Fig. 5b).

The chromatographic retention time of M455-1 was 34.20 min. The full-scan mass spectrum revealed a molecular ion ( $[M + H]^+$ ) at  $m/z$  456.2603. According to the exact mass, its molecular formula was  $C_{24}H_{33}N_5O_4$ , which contained one additional O atom and two fewer H atoms than the parent drug. The major fragment ions at  $m/z$  113.1076, 98.0842, and 70.0657 were the same as those of the parent drug. M455-1 was speculated to be

the mono-oxidated and dehydrogenated metabolite of TPN171 (Fig. 5c).

**Feces.** The total radioactive components excreted in human feces accounted for 48.60% of the dose, and TPN171 accounted for 6.88% of the dose. Combined with the HR-MS analysis, 14 metabolites were detected, of which M469 was the most abundant metabolite, accounting for 7.74% of the dose (Fig. 4c).

The retention time of M469 was 39.27 min, and the molecular ion ( $[M + H]^+$ ) at  $m/z$  470.2753 was obtained in full-scan MS. According to the exact mass, the molecular formula of M469 was  $C_{25}H_{35}N_5O_4$ , which was attributed to the addition of  $C_2H_3O$  to M2. Its major fragment ions were  $m/z$  428.2648, 141.1019, 99.0919, and 70.0658. The fragment ion at  $m/z$  141.1019 was the removed

**Table 2.** Pharmacokinetics parameters of TPN171 and drug-related components in blood and plasma after a single oral administration of [<sup>14</sup>C]TPN171 suspension to 6 healthy Chinese male volunteers (means ± SD), as analyzed using noncompartmental methods with Phoenix WinNonlin.

Parameter	TPN171		[ <sup>14</sup> C]TPN171-related components		
	Unit	Blood	Plasma	Unit	Plasma
$t_{1/2}$	h	9.42 (0.910)	9.89 (1.50)	h	16.2 (4.06)
$T_{max}$	h	1.00 (0.00)	0.667 (0.204)	h	0.750 (0.274)
$C_{max}$	ng/mL	43.9 (8.20)	72.9 (20.4)	ng eq./mL	150 (32.6)
$AUC_{0-t}$	h·ng/mL	344 (24.4)	476 (24.9)	h·ng eq./mL	1720 (28.3)
$AUC_{0-\infty}$	h·ng/mL	352 (25.2)	480 (24.6)	h·ng eq./mL	2090 (24.8)
$MRT_{0-\infty}$	h	10.9 (1.33)	10.3 (1.36)	h	21.5 (4.92)

$C_{max}$  and  $T_{max}$  were obtained from the quantified data. Based on a linear trapezoidal approximation, the area under the plasma concentration versus time curve ( $AUC_{0-t}$ ) was calculated from 0 to the last measurable time point (t). The terminal elimination rate constant ( $k_e$ ) was evaluated using the plasma concentration log-linear regression equation during the elimination phase. The half-life ( $t_{1/2}$ ) was calculated as  $0.693/k_e$ . The AUC from 0 to infinity ( $AUC_{0-\infty}$ ) was estimated as the sum of ( $AUC_{0-t}$ ) and  $C_t/k_e$ , where  $C_t$  is the concentration at the last quantified time point.

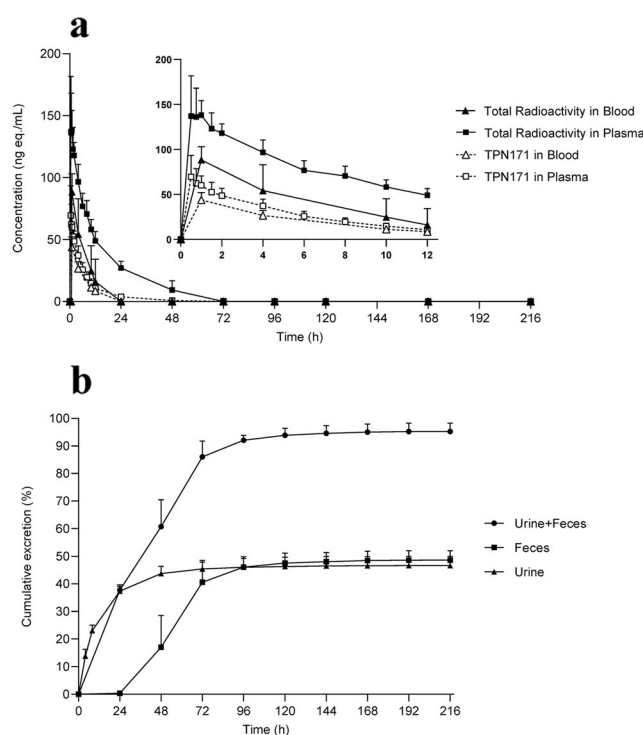


**Fig. 3** Pharmacokinetics and mass balance of TPN171 following a single oral administration of 10 mg (100  $\mu$ Ci) [<sup>14</sup>C]TPN171. **a** The concentration-time curve of [<sup>14</sup>C]TPN171-derived radioactivity and TPN171 in human blood and plasma. **b** Total cumulative radioactive dose recovered in urine and feces (%).

N-demethylated piperazine moiety. Other fragment ions were the same as those of M2. M469 was speculated to be the acetylated product of M2 (Fig. 5d).

The HR-MS analysis of other metabolites is presented in the Supplementary Information.

Incubation of TPN171 with pooled HLMs and recombinant CYP450s

In addition to the precursor drug, two metabolites were detected after incubation with the recombinant isoenzymes CYP2D6,

CYP3A5, and CYP4A11: M2 and M3-2. After the incubation with CYP2E1, one metabolite, M2, was detected, and after the incubation with CYP3A4, M1, M2, and M3-2 were detected (Table 4). According to the reduction of the parent drug and after normalization to the content in the human body, the total percent contribution of each recombinant enzyme to the generation of metabolites was calculated (Fig. 6a).

The peak area was used to calculate the slope ( $k$ ) of the natural logarithm of the amount of test drug remaining after the incubation versus the incubation time. Based on the metabolic

**Table 3.** The distribution of radioactivity from TPN171 and its major metabolites in human plasma, urine, and feces and the percent of the dose in urine and feces (%).

Metabolites	Retention time (min)	Plasma %AUC	Urine 46.61% of the dose		Feces 48.60% of the dose		Urine + Feces 95.21% of the dose
			%Urine	%Dose	%Feces	%Dose	
			TPN171	37.98–38.28	42.35	42.19	
Unknown	3.64	-	-	-	14.46	7.03	7.03
M575-1	11.67–12.34	5.27	20.02	9.33	-	-	9.33
M375	23.05–23.72	-	1.05	0.49	0.77	0.37	0.86
M473	23.65–27.46	-	1.75	0.82	1.91	0.93	1.75
TPN171M1G	27.97–28.04	14.14	2.02	0.94	-	-	1.93
M3-3	28.47–28.64	-	-	-	2.04	0.99	-
M3-1	29.27–29.41	1.12	1.30	0.61	1.74	0.85	1.46
M439-1	31.23–31.52	-	3.05	1.42	7.45	3.62	7.53
M457-1	31.29–31.49	7.05	-	-	5.12	2.49	-
M415	31.62–32.17	2.33	3.86	1.80	-	-	1.80
M457-2	32.72–32.81	-	1.72	0.80	3.70	1.80	2.60
M3-2	33.42–33.54	3.24	-	-	-	-	-
M455-1	34.20	-	6.22	2.90	-	-	2.90
M455-2	34.85–34.94	3.24	-	-	-	-	-
M6	34.87–34.97	0.96	10.62	4.95	0.70	0.34	8.46
M2	35.25–35.77	3.95	-	-	6.53	3.17	-
M1	35.41–35.73	3.24	1.90	0.89	2.01	0.98	1.87
M439-2	36.64	-	0.94	0.44	-	-	1.96
M455-3	36.94–36.98	-	-	-	3.13	1.52	-
M455-4	37.82–37.93	1.32	0.33	0.15	1.79	0.87	1.02
M439-3	38.55	2.42	-	-	-	-	-
M469	39.27	-	2.25	1.05	15.92	7.74	15.78
M7-3	39.69–39.97	4.49	-	-	14.38	6.99	-
Total		95.12	99.22	46.25	95.81	46.57	92.82

%AUC is derived from the AUC<sub>0–24 h</sub> pooled plasma; % urine is derived from the 0–48 h pooled urine sample; % feces is derived from the 0–96 h pooled fecal sample; %Dose is derived from 0–216 h of urine and fecal excretion data; -, no prominent chromatographic peak was observed in the radioactive chromatogram.

elimination of the test drug, the slope (*k*) was divided by the concentration of a certain recombinase to calculate the intrinsic clearance (CL<sub>int, x</sub>) of the test drug, and the clearance was multiplied by the enzyme abundance in native human liver microsomes to calculate the relative contribution [28, 29].

After adding ABT, a broad inhibitor of CYP450 enzymes, the remaining amount of the precursor drug increased, and the production of metabolites decreased significantly, indicating that CYP450 enzymes catalyzed the production of most metabolites. After adding ketoconazole, a CYP3A4/5 inhibitor, the amount of the precursor remaining increased significantly and the production of metabolites also decreased significantly, indicating that CYP3A4/5 was the primary enzyme that catalyzed the production of metabolites (Fig. 6b).

O-glucuronidation of TPN171 by pooled HLMs, HKMs, HIMs, HSLMs, and recombinant UGTs

Multiple reaction monitoring (MRM) mode was used to monitor the glucuronidated metabolites produced after the incubation of TPN171M1 with 13 recombinant human UGT enzymes. UGT1A7 mainly catalyzed M1 to produce M1G, followed by UGT1A9 and UGT1A10 (Fig. 7a). HSLMs, HLMs, HKMs, and HIMs were used to investigate where M1 was mainly metabolized [30–32]. Niflumic acid, an exclusive inhibitor of UGT1A9, was used for the chemical

inhibition of HLMs and HKMs. Tolcapone, a broad inhibitor of UGT1A7 and UGT1A10, was used for the chemical inhibition of HIMs and HSLMs. According to the peak area of TPN171M1G generated after incubation of microsomes with 3 μM M1, the greatest amount of M1G was produced from M1 in HIMs, followed by HKMs, HLMs, and HSLMs (Fig. 7b).

## DISCUSSION

This study reports the pharmacokinetics, mass balance, and metabolic pathway of [<sup>14</sup>C]TPN171 in humans and the primary metabolic enzymes that catalyze the production of metabolites. After oral administration of 10 mg (100 μCi) of [<sup>14</sup>C]TPN171 to 6 healthy Chinese male volunteers, TPN171 metabolites were identified in plasma, urine, and feces. Within 216 h after administration, 95.21% of the total drug-related component radioactivity was recovered in feces (48.60%) and urine (46.61%), indicating that the proportion of TPN171 and related material excreted through urine and feces was similar and that TPN171 was nearly completely excreted in humans.

Based on the high radioactivity recovery, the UHPLC-HR-MS analysis identified 22 metabolites of TPN171 in human plasma, urine, and feces, 19 of which were phase I metabolites. The main metabolic pathways were mono-oxidation, dehydrogenation, N-

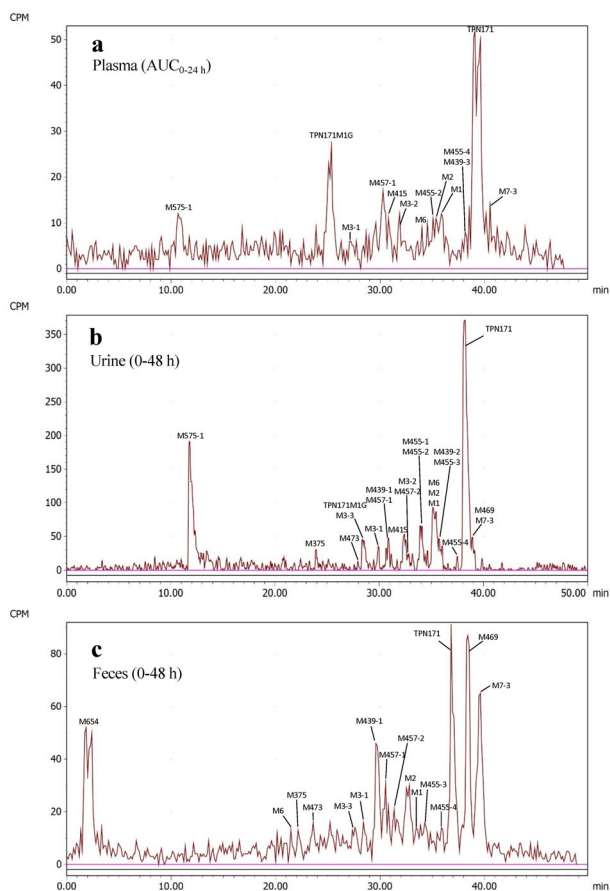


**Fig. 4** UHPLC radiochromatograms of [<sup>14</sup>C]TPN171 and its metabolites in pooled human plasma, urine, and feces. **a** Plasma (AUC<sub>0-24 h</sub>), **b** urine (0–48 h), and **c** feces (0–48 h).

dealkylation, O-dealkylation, and amide hydrolysis. Additionally, 3 phase II metabolites were identified, including two secondary glucuronides and one secondary acetylated metabolite. While the overall clearance pie was unchanged excretion (20%–26%), oxidative metabolism (~70%), and hydrolysis (~8%), indeed, no direct glucuronidation and acetylation of the parent drug played a role in the clearance of TPN171. The susceptible metabolic sites were the propyl side chain, piperazine, and diethyl pyrimidinone moieties. The biotransformation pathway of TPN171 in humans is shown in Fig. 8, and information on TPN171 metabolites detected in human plasma, urine, and feces is provided in Table 5.

In human plasma, TPN171M1G was the second most abundant metabolite, accounting for 12.14% of the total exposure to drug-related components. According to the “Technical Guidelines for Drug Metabolism Safety Tests (2020)” from the FDA, if the level of metabolites in humans is higher than 10% of the total drug exposure at a steady state, safety concerns are usually required [33]. However, phase II conjugation usually increases water solubility and decreases pharmacological activity, and thus no further evaluation is needed. Therefore, although this metabolite was detected in human plasma for the first time and exceeded 10% of the total drug exposure *in vivo*, no further tests were needed to evaluate the safety of this metabolite, but the compound is still worthy of attention [34]. In most cases, an evaluation of whether the metabolites reach 10% of the total drug-related exposure using nonradioactive pharmacokinetics studies is usually impossible, especially for drugs that produce many metabolites. This study reveals the advantages of radiolabeling technology, which accurately reflects the content of any metabolite and accurately reveals the biotransformation pathway

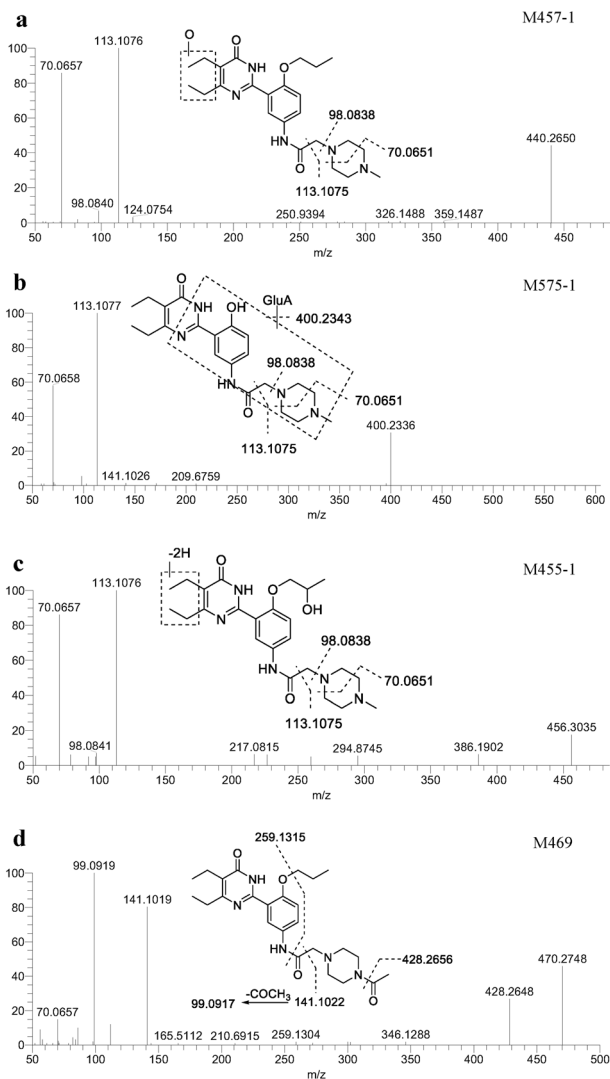


**Fig. 5** Product ion spectra and proposed fragmentation patterns of metabolites. M457-1 (a), M575-1 (b), M455-1 (c), and M469 (d).

of the drug [35]. The <sup>14</sup>C-labeled compound has constant radioactivity, with a half-life of approximately 5730 years for carbon-14 disintegration. The basic principle of radionuclide tracing is to calculate the mass balance by detecting its radioactivity.

In human urine, M575-1 was the most abundant metabolite, accounting for 9.24% of the dose. M575-1 and TPN171M1G were isomers, both of which were glucuronidation products of M1. However, compared to the concentration in plasma, the content of TPN171M1G in urine was low. According to the secondary fragmentation spectrum of M575-1, only one fragment ion generated from the loss of glucuronic acid (-176.03209 Da) was observed (Fig. 5b), and we were unable to determine whether glucuronic acid was bound to the O or N atom. Glucuronidation is the most common phase II conjugation involved in drug metabolism. Generally, glucuronidated metabolites have good water solubility and no biological activity and are easily excreted from the body [36]. The amines involved in *N*-glucuronidation are aromatic amines, fatty amines, amides, and sulfonamides. The reactivity of aromatic amines is negligible, and relatively few examples of conjugation are available. Among fatty amines, primary and secondary amines, which are more basic than other fatty amines, have a solid binding ability and more easily undergo glucuronidation [37, 38]. In addition, pyridine nitrogen and tertiary

**Table 4.** Information about the metabolites of TPN171 detected in various recombinant CYP incubation systems.

ID	Mass spectrum peak area											
	1A2	1B1	2A6	2B6	2C8	2C9	2C19	2D6	2E1	3A4	3A5	4A11
M0	1359.5	1204.6	1194.9	1415.6	1277.1	1327.4	1338.1	995.3	1052.2	662.1	660.1	1091.5
M1	-	-	-	-	-	-	-	-	-	37.7	-	-
M2	-	-	-	-	-	-	-	10.4	18.0	97.4	143.5	23.2
M3-2	-	-	-	-	-	-	-	26.5	-	100.3	115.9	24.1

-, not detected.

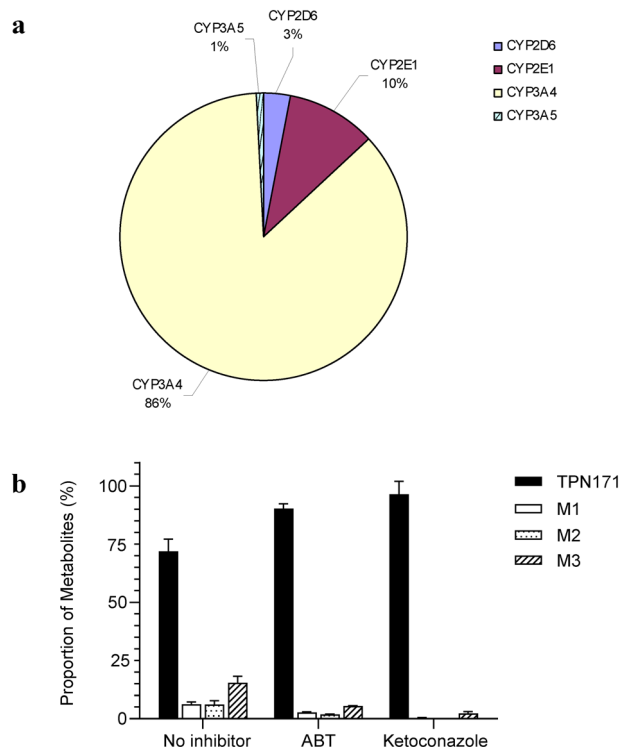


**Fig. 6** Incubation of TPN171 with pooled HLMs and recombinant CYP450s. **a** The ratio of the contribution of each recombinant enzyme to TPN171 metabolism after normalization to the abundance of each recombinant enzyme in humans. **b** Incubation of TPN171 with pooled HLMs in the presence and absence of inhibitors. The chemical inhibitors were 1-aminobenzotriazole (ABT, inhibitor of all CYP450s) and ketoconazole (CYP3A4/5 inhibitor). The results were standardized to 100%. Each column represents the average of repeated determinations.

amines with 1–2 methyl groups undergo glucuronidation to generate highly polar quaternary ammonium compounds [39]. As shown in the structure of M1, glucuronidation between the aromatic amine and secondary amine was unlikely (Fig. 1). Instead, the N with a methyl group attached to the piperazine ring underwent glucuronidation to form a quaternary ammonium compound with very high polarity. As shown in Fig. 4, the UHPLC retention time of M575-1 was earlier than that of TPN171M1G, and the polarity was higher, which validated this hypothesis.

In human feces, M469 was the most abundant metabolite, accounting for 7.99% of the dose. M469 was the acetylation product of M2. The acetylation metabolic pathway was not as common as oxidation. Acetylation is an essential metabolic pathway for drugs or metabolites containing primary amino

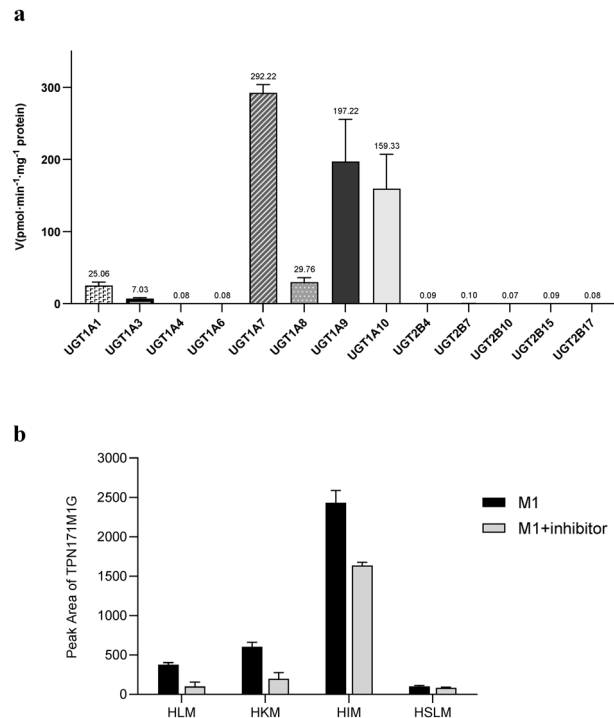


**Fig. 7** TPN171M1 O-glucuronidation by HLMs, HKMs, HIMs, HSLMs, and recombinant UGTs. **a** Glucuronidation of 3 μM M1 by 13 human recombinant UGT enzymes. Each column represents the average of repeated measurements. **b** The effect of 100 μM chemical inhibitor on the glucuronidation of 3 μM M1 in HLMs, HKMs, HIMs, and HSLMs. Niflumic acid, an exclusive inhibitor of UGT1A9, was used for the chemical inhibition of HLMs and HKMs. Tolcapone, a broad inhibitor of UGT1A7 and UGT1A10, was used for the chemical inhibition of HIM and HSLM. Each column represents the average of repeated determinations.

groups (including aliphatic amines and aromatic amines), amino acids, sulfonamides, hydrazine, and hydrazides [40]. Most phase II conjugation reactions increase the hydrophilicity and polarity. However, the polarity of M469 was reduced compared to that of the parent drug. The acetylation reaction generally deactivates foreign components in the body [41]. Most aromatic primary amines easily undergo acetylation. The N atom was aromatic after demethylation of the piperazine ring of M2, and it was speculated to undergo acetylation easily. The high amount of M469 in feces also validated this hypothesis.

Recombinase CYP450 experiments showed that CYP3A4 mainly catalyzed the production of TPN171 metabolites, and CYP2E1 and CYP2D6 were also involved in the metabolism of TPN171 to a lesser extent. The effect of the addition of the CYP3A4/5-specific

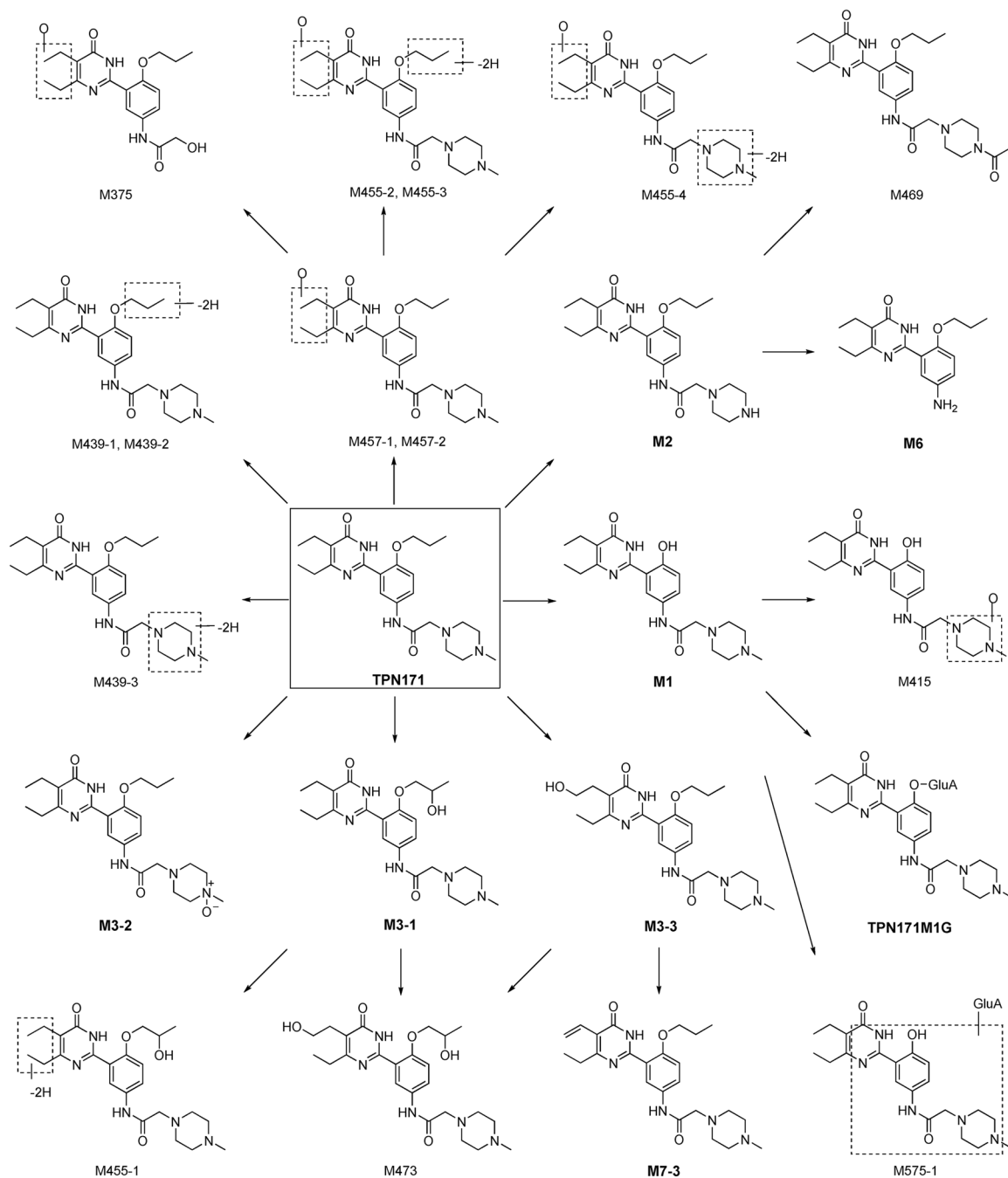


**Fig. 8** Pathway of TPN171 metabolism in healthy Chinese male volunteers. GluA glucuronic acid.

inhibitor ketoconazole to HLMs was also tested, revealing that CYP3A4 mainly mediated the production of oxidated metabolites of TPN171. In the UGT recombinase experiment, M1G was primarily produced through metabolism mediated by UGT1A7, UGT1A9, and UGT1A10. However, after comparing the metabolism of M1 in HLMs, HLMs, HIMs, and HSLMs, M1G was mainly metabolized in HIMs. The distribution and catalytic types of various enzymes in multiple tissues are different. Since glucuronidation is the primary metabolic pathway of many compounds, the structure and enzymes involved must be identified to provide information for studies of gene polymorphisms and potential clinical drug–drug interactions [42].

In conclusion, after oral administration of 10 mg (100  $\mu$ Ci) of [<sup>14</sup>C]TPN171 to 6 healthy Chinese male volunteers, TPN171 was quickly absorbed with a  $T_{max}$  of 0.667 h. Moreover, 95.21% of the administered dose of radiopharmaceutical-related components was excreted within 216 h (46.61% in urine and 48.60% in feces). In addition to the parent drug, TPN171M1G and M575-1 were the most abundant metabolites detected in human plasma and urine. M469 and M7-3 were the most abundant metabolites detected in human feces. CYP3A4 was mainly responsible for the oxidative metabolism of TPN171, and UGT1A7, UGT1A9, and UGT1A10 were mainly responsible for subsequent glucuronidation. Our study provides a better understanding of the absorption, metabolism,

**Table 5.** Information on TPN171 metabolites detected in human plasma, urine, and feces by using UHPLC-Q Exactive Plus MS.

ID	Pathway	Retention time (min)	Matrix	Formula	[M + H] <sup>+</sup> + m/z (measured)	Mass error (ppm)	Fragment ions
TPN171	Parent	37.98–38.28	P, U, F	C <sub>24</sub> H <sub>35</sub> N <sub>5</sub> O <sub>3</sub>	442.2806	-0.2	314.1867, 286.1186, 259.1315, 244.1206, 113.1073, 98.0838, 70.0651
M6	Hydrolysis	34.87–34.97	P, U, F	C <sub>17</sub> H <sub>23</sub> N <sub>3</sub> O <sub>2</sub>	302.1859	-0.1	259.1315, 244.1206, 126.0913, 81.0699
M375	[-C <sub>5</sub> N <sub>2</sub> H <sub>10</sub> ] + [2O]	23.05–23.72	U, F	C <sub>19</sub> H <sub>25</sub> N <sub>3</sub> O <sub>5</sub>	376.1859	-0.2	358.1755, 316.1281, 287.1259, 244.1068, 112.0759, 96.0809, 70.0657
M1	[-C <sub>3</sub> H <sub>6</sub> ]	35.41–35.73	P, U, F	C <sub>21</sub> H <sub>29</sub> N <sub>5</sub> O <sub>3</sub>	400.2337	-0.1	113.1073, 98.0838, 70.0651
M415	M1 + [O]	31.62–32.17	P, U	C <sub>21</sub> H <sub>29</sub> N <sub>5</sub> O <sub>4</sub>	416.2285	-0.2	329.1609, 286.1181, 259.1316, 113.1073, 98.0838, 70.0651
M2	[-CH <sub>2</sub> ]	35.25–35.77	P, U, F	C <sub>23</sub> H <sub>33</sub> N <sub>5</sub> O <sub>3</sub>	428.2650	-0.1	302.1863, 259.1315, 113.1073, 98.0838, 70.0651
M7-3	[-2H]	39.69–39.97	P, U, F	C <sub>24</sub> H <sub>33</sub> N <sub>5</sub> O <sub>3</sub>	440.2648	-0.2	284.1030, 113.1073, 98.0838, 70.0651
M439-1	[-2H]	31.23–31.52	U, F	C <sub>24</sub> H <sub>33</sub> N <sub>5</sub> O <sub>3</sub>	440.2642	-0.2	440.2653, 113.1073, 98.0838, 70.0651
M439-2	[-2H]	36.64	U	C <sub>24</sub> H <sub>33</sub> N <sub>5</sub> O <sub>3</sub>	440.2650	-0.1	440.2653, 113.1076, 98.0842, 70.0657
M439-3	[-2H]	38.55	P	C <sub>24</sub> H <sub>33</sub> N <sub>5</sub> O <sub>3</sub>	440.2635	-0.5	342.1805, 328.1646, 286.1179, 111.0920, 89.0601
M455-1	[-2H] + [O]	34.20	U	C <sub>24</sub> H <sub>33</sub> N <sub>5</sub> O <sub>4</sub>	456.2603	0.0	386.1902, 294.8756, 217.0815, 113.1076, 98.0842, 70.0657
M455-2	[-2H] + [O]	34.85–34.94	P, U	C <sub>24</sub> H <sub>33</sub> N <sub>5</sub> O <sub>4</sub>	456.2596	-0.2	369.1906, 326.1496, 284.1024, 113.1076, 98.0842, 70.0657
M455-3	[-2H] + [O]	36.94–36.98	U, F	C <sub>24</sub> H <sub>33</sub> N <sub>5</sub> O <sub>4</sub>	456.2597	-0.2	302.1854, 259.1306, 155.0813, 127.0865, 99.0918
M455-4	[-2H] + [O]	37.82–37.93	P, U, F	C <sub>24</sub> H <sub>33</sub> N <sub>5</sub> O <sub>4</sub>	456.2594	-0.2	286.1187, 127.0865, 99.0919
M3-1	[O]	29.27–29.41	P, U, F	C <sub>24</sub> H <sub>35</sub> N <sub>5</sub> O <sub>4</sub>	458.2757	-0.1	266.0798, 113.1073, 98.0838, 70.0651
M3-2	[O]	33.42–33.54	P, U	C <sub>24</sub> H <sub>35</sub> N <sub>5</sub> O <sub>4</sub>	458.2756	-0.1	371.2078, 328.1656, 286.1186, 258.1237, 113.1073, 98.0838, 70.0651
M3-3	[O]	28.47–28.64	U, F	C <sub>24</sub> H <sub>35</sub> N <sub>5</sub> O <sub>4</sub>	458.2757	-0.1	440.2656, 113.1073, 98.0838, 70.0651
M457-1	[O]	34.29–31.49	P, U, F	C <sub>24</sub> H <sub>35</sub> N <sub>5</sub> O <sub>4</sub>	458.2755	-0.2	440.2650, 124.0754, 113.1073, 98.0838, 70.0651
M457-2	[O]	32.72–32.81	U, F	C <sub>24</sub> H <sub>35</sub> N <sub>5</sub> O <sub>4</sub>	458.2752	-0.2	440.2650, 121.0642, 113.1073, 98.0840, 70.0657
M469	M2 + [COCH <sub>2</sub> ]	39.27	U, F	C <sub>25</sub> H <sub>35</sub> N <sub>5</sub> O <sub>4</sub>	470.2753	-0.2	428.2648, 141.1019, 99.0919, 70.0657
M473	[2O]	23.65–27.46	U, F	C <sub>24</sub> H <sub>35</sub> N <sub>5</sub> O <sub>5</sub>	474.2707	-0.1	456.2596, 369.1906, 326.1497, 284.1034, 113.1076, 98.0841, 70.0657
M575-1	M1 + [GluA]	11.67–12.34	P, U	C <sub>27</sub> H <sub>37</sub> N <sub>5</sub> O <sub>9</sub>	576.2653	-0.2	400.2330, 113.1073, 98.0838, 70.0651
TPN171M1G	M1 + [GluA]	27.97–28.04	P, U	C <sub>27</sub> H <sub>37</sub> N <sub>5</sub> O <sub>9</sub>	576.2656	-0.1	400.2343, 141.1022, 113.1073, 98.0838, 70.0651

HR-MS and HR-MS<sup>2</sup> acquisition tests were performed using a Vanquish UHPLC system coupled with a Q Exactive Plus mass spectrometer equipped with an ESI source. All possible metabolites were input into the inclusion list, and the MS/MS data were acquired when the target m/z ions were detected.

[GluA] glucuronidation; [-2H] dehydrogenation; [O] oxidation; P plasma; U urine; F feces.

and excretion of TPN171 in humans. These data suggest that TPN171 might become a first-line drug for the treatment of PAH.

## ACKNOWLEDGEMENTS

The research was sponsored by Vigonvita Life Sciences Co., Ltd and was partially financially supported by a grant from the National Natural Science Foundation of China (No. 81903701).

## AUTHOR CONTRIBUTIONS

YFH, JHY, HC, ZW, and XXD were responsible for analyzing samples and writing the manuscript. GHT, XMY, HQD, CYY, CY, YML, GYL, JSS, ZW, and XXD designed the scheme of this clinical study and recruited volunteers. CYY, CY, YML, and GYL were responsible for sample collection in the clinic. YL, AO, FPY, JSS, and ZW synthesized the reference substances. GHT, XMY, and HQD provided financial support.

## ADDITIONAL INFORMATION

**Supplementary information** The online version contains supplementary material available at <https://doi.org/10.1038/s41401-022-00922-6>.

**Competing interests:** GHT, XMY, and HQD are employees of Vigonvita Life Sciences Co., Ltd. The other authors have no competing interests to declare.

## REFERENCES

1. Wang Z, Jiang X, Zhang X, Tian G, Yang R, Wu J, et al. Pharmacokinetics-driven optimization of 4 (3H)-pyrimidinones as phosphodiesterase type 5 inhibitors leading to TPN171, a clinical candidate for the treatment of pulmonary arterial hypertension. *J Med Chem*. 2019;62:4979–90.
2. Qian H, Chen Q, Liang L, Zou Y, Pu H, Xin L, et al. A phase I study to evaluate the safety, tolerability, and pharmacokinetics of TPN171H, a novel phosphodiesterase type 5 inhibitor, in healthy subjects. *Drug Des Devel Ther*. 2021;15:2947–59.
3. Pan L, Guo S, Chen X, Jiang X, Shen J, Diao X, et al. Characterization of TPN171 metabolism in humans via ultra-performance liquid chromatography/quadrupole time-of-flight mass spectrometry. *J Pharm Biomed Anal*. 2019;172:302–10.
4. Sutendra G, Michelakis ED. Pulmonary arterial hypertension: challenges in translational research and a vision for change. *Sci Transl Med*. 2013;5:208sr5.
5. Schermuly RT, Ghofrani HA, Wilkins MR, Grimminger F. Mechanisms of disease: pulmonary arterial hypertension. *Nat Rev Cardiol*. 2011;8:443–55.
6. Li XM, Li T. Combined methods (formal adjusted indirect comparison, meta-analysis, and principal component analysis) comparisons of the safety and efficacy of Ambrisentan, Bosentan, and sildenafil in the patients with pulmonary arterial hypertension. *Front Pharmacol*. 2020;11:400.
7. Rai PR, Cool CD, King JA, Stevens T, Burns N, Winn RA, et al. The cancer paradigm of severe pulmonary arterial hypertension. *Am J Respir Crit Care Med*. 2008;178:558–64.
8. Buckley MS, Staib RL, Wicks LM, Feldman JP. Phosphodiesterase-5 inhibitors in management of pulmonary hypertension: safety, tolerability, and efficacy. *Drug Health Patient Saf*. 2010;2:151–61.
9. Yao A. Recent advances and future perspectives in therapeutic strategies for pulmonary arterial hypertension. *J Cardiol*. 2012;60:344–9.
10. Maurice DH, Ke H, Ahmad F, Wang Y, Chung J, Manganiello VC. Advances in targeting cyclic nucleotide phosphodiesterases. *Nat Rev Drug Discov*. 2014;13:290–314.
11. Daugan A, Grondin P, Ruault C, Le Monnier de Gouville AC, Coste H, Linget JM, et al. The discovery of tadalafil: A novel and highly selective PDE5 inhibitor. 2: 2, 3, 6, 7, 12, 12a-hexahydro-pyrazino [1', 2': 1, 6] pyrido [3, 4-b] indole-1, 4-dione analogues. *J Med Chem*. 2003;46:4533–42.
12. Ghofrani HA, Osterloh IH, Grimminger F. Sildenafil: from angina to erectile dysfunction to pulmonary hypertension and beyond. *Nat Rev Drug Discov*. 2006;5:689–702.
13. Bischoff E. Potency, selectivity, and consequences of nonselectivity of PDE inhibition. *Int J Impot Res*. 2004;16:S11–S14.
14. Gbekor E, Bethel S, Fawcett L, Mount N, Phillips S. Selectivity of sildenafil and other phosphodiesterase type 5 (PDE5) inhibitors against all human phosphodiesterase families. *Eur Urol*. 2002;1:63.
15. Duan H, Zheng J, Lai Q, Liu Z, Tian G, Wang Z, et al. 2-Phenylquinazolin-4 (3H)-one, a class of potent PDE5 inhibitors with high selectivity versus PDE6. *Bioorg Med Chem Lett*. 2009;19:2777–9.
16. Lee SK, Kim DH, Yoo HH. Comparative metabolism of sildenafil in liver microsomes of different species by using LC/MS-based multivariate analysis. *J Chromatogr B*. 2011;879:3005–11.

17. Penner N, Xu L, Prakash C. Radiolabeled absorption, distribution, metabolism, and excretion studies in drug development: why, when, and how? *Chem Res Toxicol*. 2012;25:513–31.
18. Yamada M, Mendell J, Takakusa H, Shimizu T, Ando O. Pharmacokinetics, metabolism, and excretion of [<sup>14</sup>C]esaxerenone, a novel mineralocorticoid receptor blocker in humans. *Drug Metab Dispos*. 2019;47:340–9.
19. Vincent SH, Reed JR, Bergman AJ, Elmore CS, Zhu B, Xu S, et al. Metabolism and excretion of the dipeptidyl peptidase 4 inhibitor [<sup>14</sup>C]sitagliptin in humans. *Drug Metab Dispos*. 2007;35:533–8.
20. Paulson SK, Hribar JD, Liu NW, Hajdu E, Bible RH Jr, Piergies A, et al. Metabolism and excretion of [<sup>14</sup>C]celecoxib in healthy male volunteers. *Drug Metab Dispos*. 2000;28:308–14.
21. Zheng YD, Zhang H, Zhan Y, Bian YC, Ma S, Gan HX, et al. Pharmacokinetics, mass balance, and metabolism of [<sup>14</sup>C]cvcagrel, a novel irreversible P2Y12 inhibitor in humans. *Acta Pharmacol Sin*. 2021;42:1535–46.
22. Zheng YD, Zhang H, Liu ML, Li GZ, Ma S, Zhang Z, et al. Pharmacokinetics, mass balance, and metabolism of the novel URAT1 inhibitor [<sup>14</sup>C]HR011303 in humans: metabolism is mediated predominantly by UDP-glucuronosyltransferase. *Drug Metab Dispos*. 2022. <https://doi.org/10.1124/dmd.121.000581>.
23. Hop CE, Wang Z, Chen Q, Kwei G. Plasma-pooling methods to increase throughput for in vivo pharmacokinetic screening. *J Pharm Sci*. 1998;87:901–3.
24. de Montellano PRO. 1-Aminobenzotriazole: a mechanism-based cytochrome P450 inhibitor and probe of cytochrome P450 biology. *Med Chem*. 2018;8:038.
25. Vermeer LM, Isringhausen CD, Ogilvie BW, Buckley DB. Evaluation of ketoconazole and its alternative clinical CYP3A4/5 inhibitors as inhibitors of drug transporters: the in vitro effects of ketoconazole, ritonavir, clarithromycin, and itraconazole on 13 clinically-relevant drug transporters. *Drug Metab Dispos*. 2016;44:453–9.
26. Miners JO, Bowalgaha K, Elliot DJ, Baranczewski P, Knights KM. Characterization of niflumic acid as a selective inhibitor of human liver microsomal UDP-glucuronosyltransferase 1A9: application to the reaction phenotyping of acetaminophen glucuronidation. *Drug Metab Dispos*. 2011;39:644–52.
27. Lv X, Wang XX, Hou J, Fang ZZ, Wu JJ, Cao YF, et al. Comparison of the inhibitory effects of tolcapone and entacapone against human UDP-glucuronosyltransferases. *Toxicol Appl Pharmacol*. 2016;301:42–49.
28. Achour B, Barber J, Rostami-Hodjegan A. Expression of hepatic drug-metabolizing cytochrome p450 enzymes and their intercorrelations: a meta-analysis. *Drug Metab Dispos*. 2014;42:1349–56.
29. Kawakami H, Ohtsuki S, Kamiie J, Suzuki T, Abe T, Terasaki T. Simultaneous absolute quantification of 11 cytochrome P450 isoforms in human liver microsomes by liquid chromatography tandem mass spectrometry with in silico target peptide selection. *J Pharm Sci*. 2011;100:341–52.
30. Rowland A, Miners JO, Mackenzie PI. The UDP-glucuronosyltransferases: their role in drug metabolism and detoxification. *Int J Biochem Cell Biol*. 2013;45:1121–32.
31. Masuhiro N, Shinsaku N. Tissue-specific mRNA expression profiles of human phase I metabolizing enzymes except for cytochrome P450 and phase II metabolizing enzymes. *Drug Metab Pharmacokin*. 2006;21:357–74.
32. Nakamura A, Nakajima M, Yamanaka H, Fujiwara R, Yokoi T. Expression of UGT1A and UGT2B mRNA in human normal tissues and various cell lines. *Drug Metab Dispos*. 2008;36:1461–4.
33. Schadt S, Bister B, Chowdhury SK, Funk C, Hop C, Humphreys WG, et al. A decade in the MIST: learnings from investigations of drug metabolites in drug development under the “metabolites in safety testing” regulatory guidance. *Drug Metab Dispos*. 2018;46:865–78.
34. Robison TW, Jacobs A. Metabolites in safety testing. *Bioanalysis*. 2009;1:1193–200.
35. Guideline I. Stability testing of new drug substances and products. Q1A (R2), Curr step. 2003;4:1–24.
36. Shulami S, Gat O, Sonenshein AL, Shoham Y. The glucuronic acid utilization gene cluster from *Bacillus stearothermophilus* T-6. *J Bacteriol*. 1999;181:3695–704.
37. Clarke D, Burchell B. The uridine diphosphate glucuronosyltransferase multigene family: function and regulation. In: Kauffman FC, editor. *Conjugation—Deconjugation Reactions in Drug Metabolism and Toxicity*. Handbook of Experimental Pharmacology. Vol. 112. Berlin, Heidelberg: Springer; 1994. p. 3–43.
38. Kaivosaaari S, Finel M, Koskinen M. N-glucuronidation of drugs and other xenobiotics by human and animal UDP-glucuronosyltransferases. *Xenobiotica*. 2011;41:652–69.
39. Miners JO, Mackenzie PI. Drug glucuronidation in humans. *Pharmacol Ther*. 1991;51:347–69.
40. Wang P, Shehu AI, Lu J, Joshi RH, Venkataramanan R, Sugamori KS, et al. Deficiency of N-acetyltransferase increases the interactions of isoniazid with endobiotics in mouse liver. *Biochem Pharmacol*. 2017;145:218–25.
41. Evans DAP. N-acetyltransferase. *Pharmacol Ther*. 1989;42:157–234.
42. Fisher MB, Paine MF, Strelevitz TJ, Wrighton SA. The role of hepatic and extra-hepatic UDP-glucuronosyltransferases in human drug metabolism. *Drug Metab Rev*. 2001;33:273–97.